An Experimental Method for Testing Reactivity Models: A High-Pressure Discharge−Flow Study of H + Alkene and Haloalkene Reactions

James S. Clarke,† Neil M. Donahue,* Jesse H. Kroll, Heather A. Rypkema, and James G. Anderson

Department of Chemistry and Chemical Biology, Harvard University, Cambridge, Massachusetts 02138

Received: December 2, 1999; In Final Form: March 20, 2000

Theories of barrier height control in radical−molecule reactions must be tested against data spanning a wide range in reactivity, by a method for separating multiple, correlated terms in the theories. Here we present an analysis technique designed to reveal reactant properties controlling reactivity and rate constant measurements for an extensive series of reactions where that control is very much in doubt. The measurements were made with a new high-pressure flow experiment designed specifically to facilitate the study of multiple radicals. The derivative technique consists of graphically analyzing partial derivatives of modeled barrier heights, using measured barriers and reactant properties. We use this technique to uncover the governing parameters for hydrogen atom abstraction reactions, which are dominated by an essentially ionic excited state of the reactants. More generally, multiple excited states contribute to barrier formation, with different states dominating for different classes of reactions. The new experimental apparatus is a significantly more flexible (and much smaller) version of our original high-pressure flow system. In this case, we use hydrogen atoms as the attacking radical, enabling a study of hydrogen atom addition to alkenes, where reactivity may be controlled by ionic states, singlet−triplet splittings, reaction enthalpy, or a combination of these factors. By using hydrogen atoms, we eliminate potentially confounding influences on the ground state, and by selecting a series of alkenes and haloalkenes to systematically vary ionization potential, singlet−triplet splittings, and π-electron density, we lay the foundation for an extensive study of barrier height control for this reaction class. The data presented here include the first temperature-dependent measurements for 9 of the 13 reactions studied.

Introduction

Radical−molecule reactions lie at the heart of a very broad range of chemical systems. Examples include the formation of carbon−carbon bonds in organic synthesis,[1−3] the attack and subsequent breakdown of DNA and proteins,[2,4,5] the high temperature combustion of fuels,[6,7] the catalytic depletion of ozone,[8,9] and the photochemical formation of smog.[10,11] Because these reactions involve the interaction of an open-shell system with a closed-shell system, there is the potential for reaction barriers to be very low, but barriers will in general be present. Consequently, reactivity in homologous series of radical−molecule reactions spans a huge range. Reaction probabilities for exothermic reactions vary from once per collision to immeasurably low, spanning at least 12 decades. This variability has profound implications for many natural and artificial systems, and understanding it is of the highest importance.

In full, understanding radical−molecule reactivity involves understanding both what controls the morphology of the potential energy surface (PES) and the reaction dynamics on that surface. A sequence of radical−molecule potential energy surfaces is shown in Figure 1, which depicts a smooth transition from barrierless additions to concerted bimolecular reactions with a simple barrier. Rate constants for different reaction types will have different contributions from enthalpy (the PES) and entropy (the dynamics). As much as possible, we aim to separate these two components. When considering factors that form the potential energy surface, the simplest classes of reactions are atom transfers and additions with a significant barrier and a long-lived adduct. In these cases, thermal equilibrium holds along the reaction coordinate, and canonical transition state theory reasonably describes the reaction dynamics. It is then possible to consider what controls these barriers without undue complications associated with the dynamics.

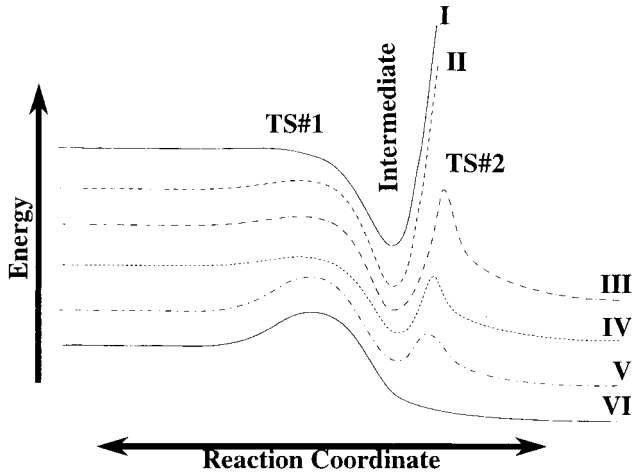

Figure 1. The evolution of potential energy surface morphology for radical−molecule reactions. At the extremes are barrierless additions (**I**) and simple atom transfers (**VI**). Between are additions with barriers (**II**) and several types of reactions with multiple transition states (**III**−**V**).

* Corresponding author.
† Present address: Laboratorium für Organische Chemie, ETH Zürich, Universitätstrasse 16, CH-8092 Zürich, Switzerland.

10.1021/jp9942421 CCC: $19.00
Published on Web 05/13/2000

Our approach has been to focus on the evolution of reactivity in a series of reactions; by studying a sequence of reactions we can isolate particular boundary conditions driven by molecular properties of the reactants. A wide range of reactivity must be covered, and the reactions must be chosen so that particular details of competing theories can be probed. In general, these conditions mean that reactions involving a manifold of radicals reacting with a manifold of molecules must be studied within a given reaction class. It is also necessary to cover a wide range of pressures and temperatures, especially when exploring the effects of dynamics and multiple transition states. Furthermore, the data must be analyzed in a manner that facilitates comparison with the theories. Parameters associated with the fitting of data should be physically meaningful, and the subsequent analysis should clearly show the role of various terms in the theoretical description.

These considerations motivate our experimental design and our approach to data analysis. We have previously described in detail the fundamental principles of high-pressure flow (HPF) kinetics.[12] Our original system can be operated over a wide range of temperatures (170−400 K)[13] and pressures (1−600 Torr),[14] but has been confined to the study of OH radicals. So far, we have relied on literature data to provide constraints for radicals other than OH. Furthermore, it was designed to ensure well-developed laminar and turbulent flow, primarily through the use of a 600-L dwell chamber and a 5-m-long prereaction zone. Consequently, it is difficult to replicate.

When assessing the evolution of reactivity, we always analyze all data, our own and that from the literature, with a consistent approach. For the reasons already described, we avoid simple Arrhenius fitting for atom-transfer reactions. Arrhenius fits imply a direct relationship between the activation energy (Arrhenius slope at a given temperature) and the actual reaction barrier, whereas the modified forms divide the effect of the barrier between a Boltzman term and a T^n power dependence. We use a function that explicitly retains the translational and rotational partition functions of the reaction, plus a few critical vibrational partition functions.[15] We have recently further refined this to include tunneling.[16]

Finally, when we do establish consistency between predicted and observed reactivity, we need to quantitatively assess what is driving the variations we see. In particular, we need to be able to separate the various properties of reactants and products that constrain the transition state to determine which properties are truly controlling and which are less influential.

In this paper, we will address these issues. We shall describe a new experimental system designed to probe reactions involving a wide range of radicals, including atoms and OH, in a much smaller package that does not depend on a well-developed velocity profile. We shall also develop the formalism for a derivative analysis technique designed to describe the properties influencing reactivity. To illustrate this technique, we shall analyze the results of our earlier study, demonstrating the controlling role of ionic states in many H atom transfer reactions.[17] Finally, we shall present new measurements for a large series of H−alkene addition reactions.

We choose H atom additions to extend our work on barrier height control from atom transfer to addition reactions, using a radical with few complicating factors in the far field. In studying addition reactions, we are seeking the transition in barrier height control from ionic to covalent interactions; currently, there is some ambiguity about the processes that control barrier heights in radical−molecule reactions in general. Barrier height control by both covalent[18−20] and ionic[13,17] excited states has been proposed. Our objective is to develop a theoretical formalism that simply describes a smooth transition from one extreme to the other. In a companion paper,[21] we shall employ the data and methods presented here to assess the relative contributions of both factors to this set of addition reactions.

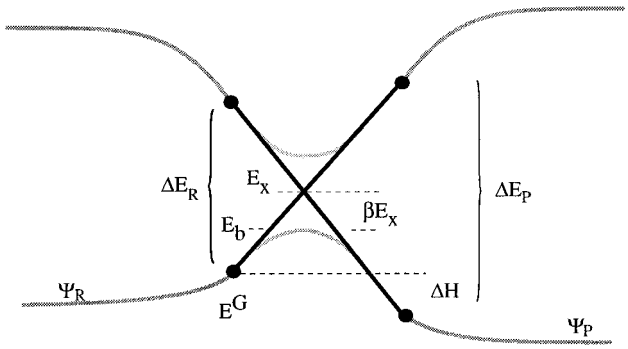

Figure 2. The two-state crossing model. The ground and the excited state of reactants and products cross. The energy gaps ΔE_R, ΔE_P , and ΔH are shown. These gaps establish the crossing height E_X (see eq 1). Strong quantum mechanical mixing of these states lowers the energy of the adiabatic surface to give the barrier height, E_b.

Testing Theories

Theoretical Approach. Our goal is to understand and predict the progression of reactivity in radical−molecule reactions. Our approach is to use a two-state curve-crossing model constrained by properties of the separated reactants and products and tested against measured barrier heights. Although this approach has been discussed in detail in previous work,[13,17] we briefly highlight the model here.

In all radical−molecule reactions, the reactants and products must be described by two separate wave functions. This requires that the transformation from reactants to products corresponds to a curve crossing,[20,22] where the ground state of the reactants maps into a promoted state of the products and vice versa. The relevant promoted states are assumed to be the excited states that couple most strongly to the ground state on the opposite side of the reaction barrier. Two types of excited states can be chosen to constrain the curve crossing: covalent excited states resulting from the singlet−triplet transition of the bonds being broken and formed in the course of the reactions, and ionic states resulting from the transfer of an electron between the frontier molecular orbitals (FMOs) of the two reacting species. The initial energies of both surfaces can be ascribed to experimentally determined properties (i.e., bond strength, ionization potential, etc.), and the subsequent energetic evolution of each state can be modeled in the far field.

The central assumption of this model is that the energies of the ground and excited states evolve linearly over an extended distance near the transition state (see Figure 2). Although such an assumption is an oversimplication, it permits a simple description of the curve crossing. Deviations from a linear crossing can easily be accommodated,[23] but as long as the general shape does not vary from reaction to reaction, the exact shape will not influence barrier evolution. Assuming a linear crossing bounded by the energies of the ground and excited states of the reactants and products, we find:

$$E_X = E_R^G + \frac{\Delta E_R(\Delta E_P + \Delta H)}{\Delta E_R + \Delta E_P} \qquad (1)$$

where E_R^G is the reactant ground-state energy, ΔH is the

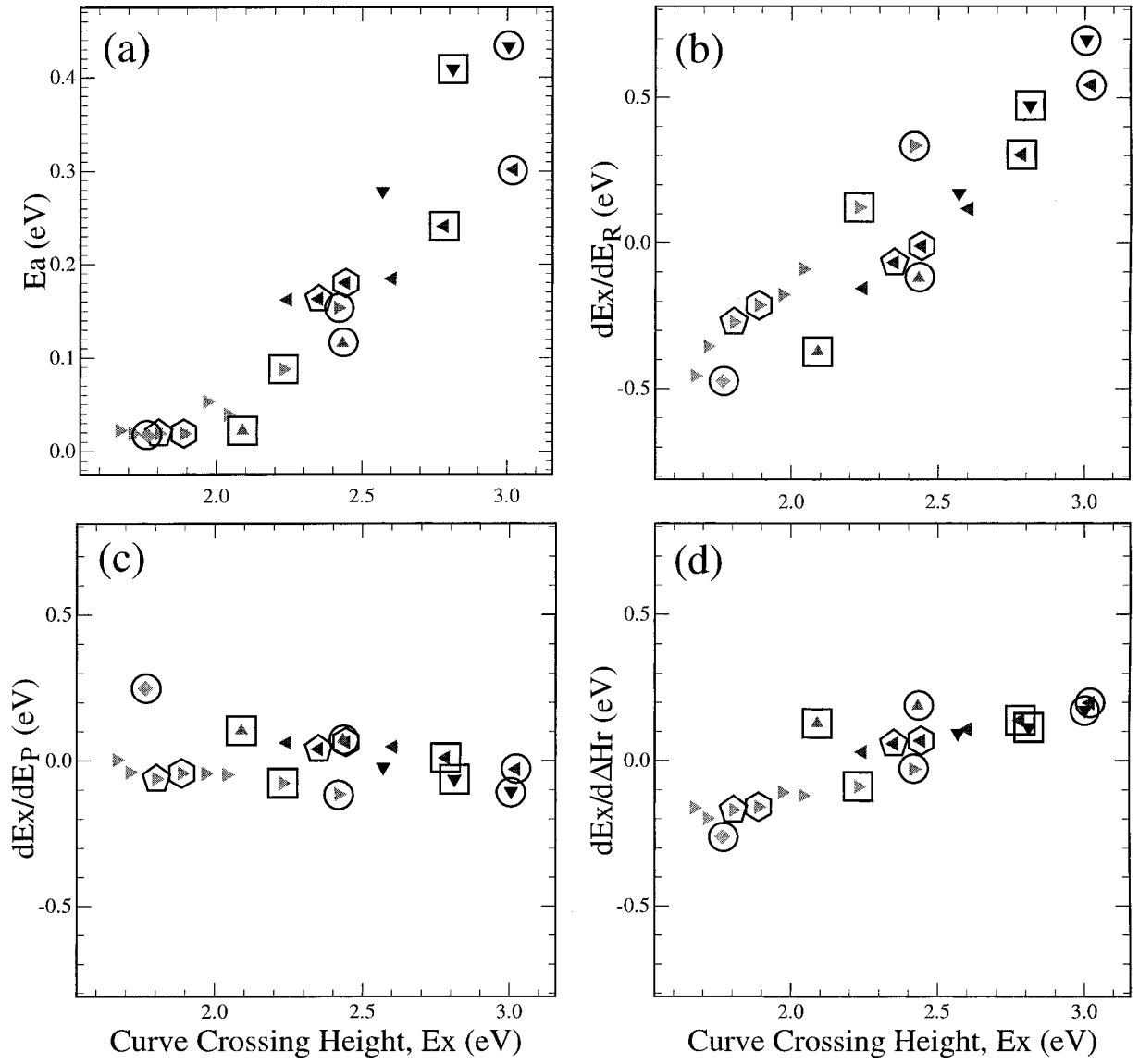

Figure 3. Derivative analysis for H atom transfers by H (downward-facing triangles), O (left-facing), OH (right-facing), Cl (upward-facing), and F (diamond) from a series of alkanes, including methane (open circle), ethane (square), and cyclohexane (hexagon). (a) Predicted crossing heights versus observed barriers. (b) Variation in the predicted crossing height driven by variations in reactant excited (ionic) state energies. (c) Variation driven by product excited state energies. (d) Variation driven by reaction enthalpy, which shows quantitatively that reactant excited-state energies dominate barrier height evolution in these reactions.

reaction enthalpy, and ΔE_R and ΔE_P are the energies of the reactant and product excited states, respectively. Most radical−molecule reactions are strongly coupled; the ground and the excited states strongly mix, splitting the states into two adiabatic surfaces. Thus, the barrier height to reaction is some fraction of the curve-crossing height and is given by

$$E_b = E_X(1 - \beta) \tag{2}$$

where β represents the degree of coupling between the excited states. At this point, the construction of the two-state model is complete.

We shall use this model in two interrelated ways: one is prognostic and one is diagnostic. At this point, our prognostic goal is to predict the evolution in barrier heights for a series of reactions. As we have shown previously,[17] the measure of success or failure at this level is the ability to simultaneously describe the evolution of radical and molecule reactivity. For example, a test of predicted crossing heights versus observed activation energies for H atom transfers from our previous work is shown in Figure 3a. The predictive success of this model is far greater than others constrained by either singlet−triplet states or Marcus-type reaction enthalpy relationships. Here we are interested not in closely reproducing individual values but rather in the overall relationships that validate or refute the different models. This need to study many reactions involving multiple molecules and radicals is a major motivation for our experimental design, as described later.

Having established the validity of our model with this prognostic test, we can develop diagnostic tools to assess which of many physical factors (boundary conditions or constraints to the model) actually controls reactivity, or to discover the transitions from regimes defined by dominance of one factor to regimes defined by dominance of another factor. These tools are defined later; they consist of partial derivatives of the model with respect to the various boundary conditions, coupled with graphical depictions of how the model output (i.e., the barrier height) varies with respect to those boundary conditions. By focusing on measurable properties of reactants and products as

constraints, we sacrifice direct connection to ab initio quantum mechanics but gain insight rooted in observable chemical properties. It is the correlation of those properties that motivates studies that include a wide range of molecules and radicals.

The diagnostic results can in turn be fed back into a refined prognostic model, now with the aim of accurately predicting individual barrier heights. The model is constructed so that various terms correspond to various configuration interactions associated with the transition state. By identifying the important terms, we can discover where to focus our efforts at accurate calculation. This topic will be described in subsequent publications.

Derivative Analysis. Now we turn to the diagnostic application. The success of Figure 3a strongly suggests that eq 1 correctly describes barrier height evolution in these reactions, but it does not show which terms in eq 1 actually drive that evolution. Correlative plots of measured barrier height versus the individual components of barrier height (for example, ΔH) do not provide this ability, though they are frequently used as if they do. The problem is that there are multiple boundary conditions in eq 1, each of which changes for each reaction in a set. This covariance obscures the role of individual terms. However, the partial derivative of E_b with respect to each term can isolate the individual boundary conditions. This derivative is given by

$$\frac{dE_b}{d\,rxn} = \frac{\partial E_b}{\partial(\Delta H)} \cdot \frac{d(\Delta H)}{d\,rxn} + \frac{\partial E_b}{\partial(\Delta E_P)} \cdot \frac{d(\Delta E_P)}{d\,rxn} + \frac{\partial E_b}{\partial(\Delta E_R)} \cdot \frac{d(\Delta E_R)}{d\,rxn} + \frac{\partial E_b}{\partial \beta} \cdot \frac{d\beta}{d\,rxn} \quad (3)$$

The derivative of E_b with respect to each term is multiplied by the variability of that term over the series of reactions, which is represented abstractly by the term "d rxn". To compare the role of each term, this variability is taken to be the deviation from the average; for example,

$$\frac{d(\Delta H)}{d\,rxn} = (\Delta H_i - \langle \Delta H \rangle) \quad (4)$$

where ΔH_i is the enthalpy for a particular reaction and $\langle \Delta H \rangle$ is the expectation value for the series. Thus, the dependence of barrier height on reaction enthalpy within the two-state model is given by

$$\frac{\partial E_b}{\partial(\Delta H)} \cdot \frac{d(\Delta H)}{d\,rxn} = \frac{E_R(1-\beta)}{E_R + E_P}(\Delta H_i - \langle \Delta H \rangle) \quad (5)$$

Analogous derivatives can be formed for each term.

We can apply this approach to the atom transfer case shown in Figure 3a. This case is relatively simple, where the excited state is clearly associated with an ionic state of the separated reactants and products, so we need only consider three terms; they are, the reactant and product ionic state energies and the reaction enthalpy. We will confine ourselves to analyzing the crossing height because the coupling term β remains nearly constant over this series.[17] The simplest approach is to perform a local analysis, using the mean derivatives to calculate a single sensitivity of the crossing height to each parameter. For example,

$$\frac{\partial E_x}{\partial(\Delta E_r)} = \frac{\langle \Delta E_p \rangle (\langle \Delta E_p \rangle + \langle \Delta H \rangle)}{(\langle \Delta E_p \rangle + \langle \Delta E_r \rangle)^2} \quad (6)$$

For this system, the sensitivities are: $\partial E_x/\partial(\Delta E_r) = 0.44$, $\partial E_x/\partial(\Delta H) = 0.31$, and $\partial E_x/\partial(\Delta E_p) = 0.11$. The system is sensitive to both reactant excited state energy and reaction enthalpy, and insensitive to product excited state energy. Note that this analysis is only valid in the local regime of asymmetric reactions with relatively low reactant excited state energies, such as those described here. This local derivative analysis cannot be used in this simple way for a qualitatively different reaction like ethyl + HBr, where the product excited state is much lower than the reactant excited state.

The sensitivities alone do not show what actually drives the barriers; to discover this driving force, we must multiply by the actual variation in the boundary conditions, as shown in eq 3. The final three panels of Figure 3 show the result. Each panel shows one of the three derivatives plotted against the calculated crossing height. The range of the ordinate and abscissa on each plot is the same, so the total variability seen in Figure 3a is covered by each subsequent plot. Although it is necessary for a successful theory to produce a tight correlation between the predicted and observed barriers, such as the one shown in Figure 3a, it is not necessary that the individual terms be tightly correlated with the final result. Any contribution near the top or bottom of any one of these plots (i.e., far from 0) drives a given crossing far from the mean value. However, it turns out that there is a tight correlation and the barriers are driven by a single term. The crossing heights are driven almost entirely by the reactant excited-state energy (Figure 3b), with small counterbalancing contributions from the product excited state (Figure 3c) and the reaction enthalpy (Figure 3d). This result supports the more qualitative conclusion to this effect in our earlier work.[17]

Within this broad picture, certain subtleties emerge; for instance, there is a significant contribution lowering barriers for OH reactions from both reaction enthalpy and the product excited state. Figure 3b shows that reactant excited-state energy alone is forcing a somewhat (0.15 eV or so) higher barrier than is observed, and the other two terms drive the barrier down to that observed and plotted in Figure 3a.

A crucial part of this anaysis is that it is conducted with multiple molecules (alkanes in this case) and radicals (H, O, F, Cl, Br, and OH). The derivatives are performed in nature, and the variability associated with radical properties breaks degeneracies associated with the molecules.[17] Exploiting this consideration by facilitating multiple radical measurements is a key design constraint in the following experimental discussion.

Designing an Experiment

For the atom transfer case just presented, the two-state model we have employed succeeds in describing the observed barrier height trends. In that analysis, we combined literature data for atom−alkane reactions with our own data for OH−alkane reactions. By reanalyzing the literature data with a consistent method grounded in transition state theory, we were able to accommodate the different temperature ranges covered by the available data without biasing the barrier height determination. However, our inability to extend the atom−alkane database in both temperature range and the number of reactions was a limitation. Nevertheless, the case for ionic state control by the reactants, as already presented, is compelling.

Our interest at this point is to extend this treatment to different reaction types, including radical additions and reactions controlled by product excited states. In addition, we seek the transition from a regime where barriers are controlled by ionic excited states to one where barriers are controlled by covalent excited states (singlet−triplet splitting). In such a transition

regime, more than one excited state will necessarily influence barrier heights. The model just presented can be extended to cover multiple excited states, and the derivative analysis technique can be extended as well. The scarcity of data, especially for a range of radicals, is far more severe for addition reactions than for the relatively well-studied H atom abstractions. Furthermore, we have shown that it is vitally important to consider both a range of molecules and a range of radicals when testing reactivity theories; variability of radical reactivity is often the key to eliminating otherwise vexing correlations in the physical parameters constraining these theories. For these reasons, we need to extend the design of our high-pressure flow system to accommodate detection strategies other than laser-induced fluorescence.

We have already seen at least one case where multiple ionic states must be considered to understand the observed barrier. When OH attacks cyclopropane, the spatially extended second-highest molecular orbital and the energetically favored highest molecular orbital both contribute to the adiabatic reaction barrier. The result is a much higher barrier than one would predict with a simple two-state model bounded by the first ionic state of cyclopropane.[13] A similar situation must exist for competition between ionic and singlet−triplet excited states. The correct first-order picture of atom transfer to an electrophilic radical is a crossing bounded by ionic states (*not* a polar transition state), possibly with a perturbation by molecular triplet states. For other systems, such as the addition of alkyl radicals to alkenes, the correct first-order picture is almost certainly a curve crossing bounded by the molecular singlet−triplet splitting, with a perturbation from the ionic states (a polar effect).[18,19] Our goal is to find the transition from one regime to the other. Drawing from our past experience, we will need to measure rate constants for much more than OH radical reactions.

To meet this goal we chose to study a series of H atom additions to alkenes and haloalkenes. This series provides the necessary characteristics for an analysis of barrier height evolution. Several molecular properties vary in this reaction set, including ionization potential, singlet−triplet splitting, and the π-electron density on the reactive carbons. Each property affects a boundary condition of the two-state crossing, and therefore, influences barrier height. The H atom is moderately electrophilic (EA = 0.75 eV); it is well placed to probe the transition from ionic to singlet−triplet control, but the data base for H atom additions is sparse, necessitating measurement of rate constants for a wide range of reactions.

A final advantage of H atoms in this case is to avoid the complicating influence of prereactive complexes formed between alkenes and other radicals. For example, the reactivity of many alkenes and haloalkenes with the hydroxyl radical has been studied, with rate constants spanning 3 orders of magnitude at room temperature.[24,25] These reactions show complicated pressure and temperature dependencies resulting from the formation of dipole-induced dipole complexes, which lower the transition-state energies below the reactant energies.[25,26] In addition, complexes resulting from the *p*-orbital mixing of the halogen atoms with π-electrons have been examined theoretically for the reactions of F and Cl with ethene.[27,28] For each case, the presence of the complex masks the height of the barrier to addition and complicates an assessment of the processes that control reactivity. To focus attention on the transition-state energy, we need to eliminate the complex. Hydrogen atoms fulfill this need; H does not have a dipole, nor is it significantly polarizable.

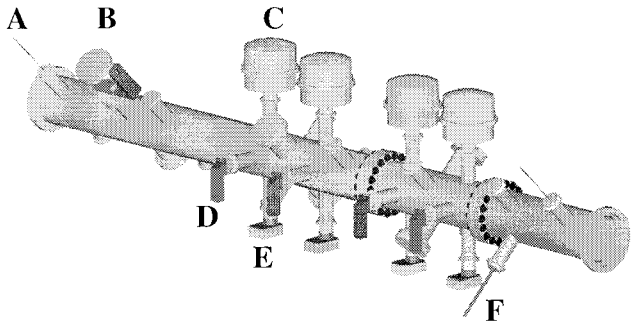

Figure 4. Schematic diagram of the high-pressure flow system (HPFS) used for measuring the rate constants of atom−molecule reactions: (A) 30 kΩ thermistor (also at end); (B) microwave plasma for the generation of hydrogen atoms; four resonance fluorescence axes comprised of (C) a lamp housing for the generation of Lyman-α light, (D) a photomultiplier tube for the detection of hydrogen fluorescence, and (E) a photodiode for the measurement of lamp flux; and (F) a Pitot-tube to measure the velocity of the core.

Nevertheless, the reaction of H + alkene is still an addition reaction; dissociation of the alkyl adduct to reactants can be competitive with formation of a thermalized adduct. Competition between dissociation and thermalization is an unwelcome complication in experiments designed to probe barrier height evolution. Experimentally, a wide pressure range is needed to constrain the reaction mechanism and to ensure that conclusions about barriers are based on data taken at the high pressure limit. Finally, one must vary temperature over a wide enough range so that imprecision of the data does not obscure any temperature dependence.

In total, we have measured the rate constants for 12 H + alkene and haloalkene reactions between 298 and 370 K, over a pressure range of 20 to 65 Torr (for a subset of reactions). The alkenes are propene, isobutene, 2-ethyl-1-butene, *cis*-2-butene, *trans*-2-butene, 2,3-dimethyl-2-butene, cyclopentene, cyclohexene, and *cis*/*trans*-3,4-dimethyl-3-hexene, and the haloalkenes are *trans*-1,2-dichloroethene, *cis*/*trans*-1,2-dibromoethene, and tetrachloroethene. These data enable an extensive analysis along the lines presented herein. That analysis is very involved, including development of a formalism describing a mixed excited state in the two-state model and subsequent derivative analysis including this mixed state. Consequently, the analysis is presented in a companion paper.[21] The rest of this paper will focus on describing the new experimental system and data.

Experimental Method

The high-pressure flow technique and analysis methods used in this work are described extensively in the literature.[12,13,29] One characteristic of the method is the presence of multiple detection axes for the radical. This multiplicity eliminates the need for a movable injector, because multiple reaction times are observed simultaneously, and greatly reduces the duration of each experiment while substantially improving the precision. However, this method requires multiple copies (at least four) of any detection scheme, and the original experiment was designed solely for laser-induced fluorescence. So, to measure atom−molecule rate constants, we built a second high-pressure flow system (HPFS) that can accommodate multiple resonance fluorescence (RF) axes. This instrument is shown in Figure 4, and individual components are labeled. Two primary changes warrant emphasis: (1) This flow tube is much shorter than that previously used in this laboratory for the measurement of rate constants. The shorter tube greatly reduces the thermal mass of

the experiment, facilitating temperature-dependent studies. (2) Although RF is used for the detection of H atoms, the axis design permits swift switching among RF, laser-induced fluorescence (LIF), and absorption [Fourier transform-infrared (FTIR), cavity ringdown, etc.] measurements; multiple radicals can now be studied easily. The procedure for measuring a rate constant, however, is essentially unchanged and will be only briefly reviewed here.

This HPFS consists of a 3.5-m long, 12.36-cm diameter stainless steel pipe through which passes a flow of nitrogen gas. The first 2 m of the flow tube allow for mixing and development of the carrier gas flow profile. This mixing region is followed by a 1.5-m detection region consisting of a radical source for the production of H atoms (B in Figure 4) and four RF axes for their detection. A 400 standard liter per minute (slm) gas flow controller (MKS) regulates a constant flow of nitrogen gas into the tube. System pressure is measured with a 300 Torr capacitance manometer slightly upstream of the detection region. The core velocity is measured following the fourth RF axis using a pitot-static tube (F in Figure 4) attached to a 0.2 Torr differential capacitance manometer (MKS, 0−10 V output). For most experiments performed here, pressure is held constant at 50 Torr while the velocity is varied from 500 to 1200 cm/s by controlling the flow of carrier gas into the system. These flow conditions result in turbulent flow profiles corresponding to Reynolds numbers of 2600−6200. Although the flow profile is not fully developed, the core velocity is nearly constant (through the measurement section the core velocity accelerates by ∼5%). To first order, the effect of this evolution is to slightly change the advection time between each axis, and this effect can be accommodated easily in the data analysis.

Hydrogen atoms are prepared in a sidearm radical source (B in Figure 4). Trace amounts of H_2 in argon are passed through a microwave plasma to generate H atoms, which are then injected into the center of the carrier gas well mixed with excess (XS) reagent. As with OH kinetics in the original HPFS,[12] the system runs in a "core flow" mode—the H atoms are not well mixed in the flow but instead are localized (and measured) in the core. Slow radial diffusion (and an essentially flat velocity profile) ensures that the advective time scale is correctly defined by the core velocity and axial distance.

The RF axes are spaced unevenly along the flow tube in two groups of two to more precisely measure both the overall slope in the radical and any unwanted curvature. Each RF axis is composed of a lamp housing to generate Lyman-α light (121.6 nm), a photomultiplier tube (PMT; RSI) perpendicular to the lamp to measure fluorescence, and a photodiode (Hamamatsu, KBr cathode) opposite the lamp to monitor lamp flux (shown in C−E in Figure 4, respectively). The sealed lamp contains ∼ 4 Torr of Ne, which serves as a bath gas. A sidearm to the lamp contains UH_3, which evolves hydrogen gas when heated. The lamps are kept optically thin (i.e., there is no Lyman-α absorption within the lamp). In addition, optical baffles on both the lamp and PMT help to reduce scattered light and limit the solid angle of atom detection to the center 8 cm^3 of the flow tube. By normalizing the PMT signal to measured lamp flux, the influence of absorbing species on the measured hydrogen fluorescence is minimized. A typical axis signal for the course of an experiment is shown in Figure 5. A more extensive discussion of the Lyman-α lamps method can be found in the literature.[30,31]

The XS concentration is determined with calibrated flow controllers. The flow of excess reagent divided by the flow of carrier gas gives the mixing ratio in the tube (once the reagent becomes well-mixed). When multiplied by the density of the gas in the flow tube, this ratio gives the reagent concentration. Reagent bulbs are carefully prepared mixtures of XS in N_2. The XS reagent is mixed into the carrier flow well upstream of the flow tube. Mixing within the tube has been verified by measuring the radial concentration profile of O_3 by ultraviolet (UV) absorption with a long-path White cell. Under our experimental conditions, no radial concentration gradient in the XS concentration is observed.

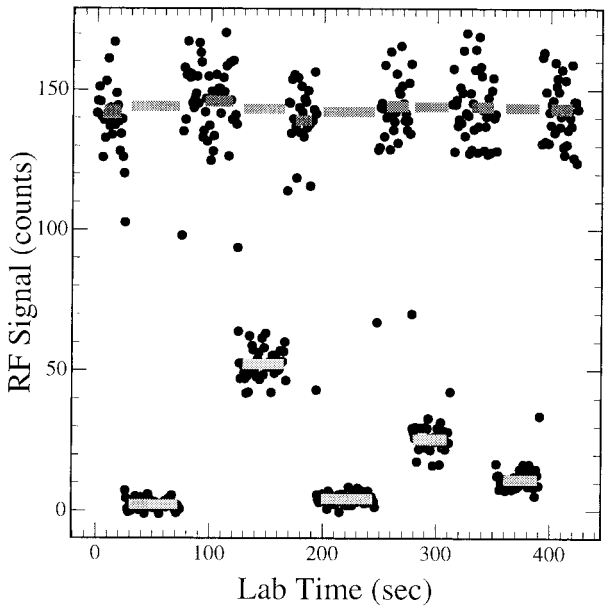

Figure 5. The H atom RF signal (axis 4) during the course of a run. Five separate reagent concentrations are established, with zero conentration intervals between each. Data are averaged as indicated by the horizontal bars, and surrounding zero concentration intervals are averaged again to provide a reference for each of the five data points. Reagent concentrations are staggered to prevent errors associated with secular drifts in signal.

For this experiment, the instrument is operated at ambient and elevated temperatures (295−370 K). System temperature is measured prior to (A in Figure 4) and following the detection region using two 30 kΩ thermistors. The carrier gas is heated in a cylindrical heater manifold (3" o.d. × 8" long), located between the carrier gas flow controller and the flow tube. Four 300 W cartridge heaters (Watlow, 1/8" × 3") are positioned perpendicular to the flow in the heater manifold. With these heaters, temperatures in excess of 370 K can rapidly be achieved for flow rates of 360 slm. In addition, the flow tube is wrapped with 12 15" flexible heaters (Watlow, total power 2 kW) and is heavily insulated. This insulation keeps axial and radial temperature deviations in the detection region at <1 K.

The procedure for obtaining a rate constant on this instrument is similar to that described previously.[13] Prior to and following a measurement, the background fluorescence is measured. During a measurement, the XS reagent is cycled on and off five times at various concentrations while H atom decay is monitored at each axis (Figure 5). The radical signal is then plotted as a function of XS concentration for each axis (Figure 6) and the log−linear slopes are determined with a weighted fit. The resulting slopes are plotted versus reaction time and again fit with a weighted linear fit, yielding the rate constant (Figure 7). We apply a small correction (<5%) when converting axial distance into reaction time to account for the developing velocity profile. With this experimental method, a rate constant

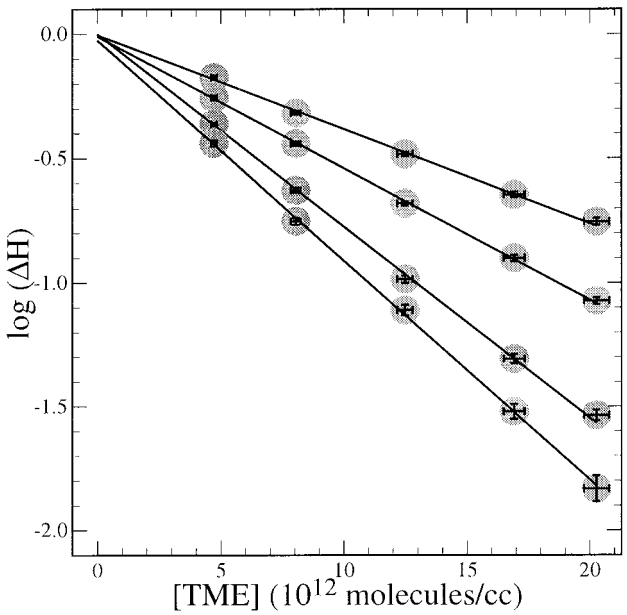

Figure 6. The log of RF signal versus reagent concentration for each axis. Note the two decades of log-linear decay and tightly grouped intercepts.

can be measured in the span 5−10 min with very high (2%) precision, as shown.

Materials. A liquid nitrogen boil-off source (99.999%) was used without further purification for the HPFS carrier flow. A mixture of 0.2% hydrogen gas in UHP argon (Matheson) was used for the H atom source. Ethene (Matheson, 99.999%), propene, isobutene, *cis*-2-butene, and *trans*-2-butene (all from Aldrich, 99%) were received in compressed gas cylinders and used without further purification. Cyclopentene (Aldrich, 99%) was received as a liquid inhibited with 0.1% hydroquinone, and cyclohexene (Aldrich, 99%) was received as a liquid inhibited with 0.01% 2,6-di-*tert*-butyl-4-methylphenol. Both were purified several times by the freeze-pump−thaw technique. It is assumed that little inhibitor was present in the reagent bulbs. Furthermore, the reactivity of H atoms with the inhibitors was assumed to be low in comparison with the H−alkene reactivity. Tetrachloroethene (Aldrich, 99.99%) *trans*-1,2-dichloroethene (Aldrich, 98%), 2,3-dimethyl-2-butene (Aldrich, 99%), and 2-ethyl-1-butene (Aldrich, 98%) were purified by the freeze-pump−thaw technique. 1,2-Dibromoethene (Aldrich, 98%) and 3,4-dimethyl-3-hexene (Aldrich, 98%) were received as cis/trans mixtures, and were also further purified.

Results

Pressure Dependence. Additions involve the formation of a stable intermediate species, and thus may show complicated behavior with respect to temperature and pressure. For example, the potential energy surface for the H + ethene reaction is shown in Figure 8(a). The reaction enthalpy is determined from experimental heats of formation,[32,33] whereas the barrier height to reaction is constrained by temperature-dependent measurements at high pressures.[34−36] The first step of this reaction is the addition of the H atom to a π-bonded carbon, producing a highly energized adduct; that is,

$$H_2C=CH_2 + H \rightleftharpoons H_3C\dot{C}H_2^* \qquad (7)$$

The adduct formed by reaction 7 can dissociate back to reactants or be collisionally deactivated to products (an alkyl radical); that is,

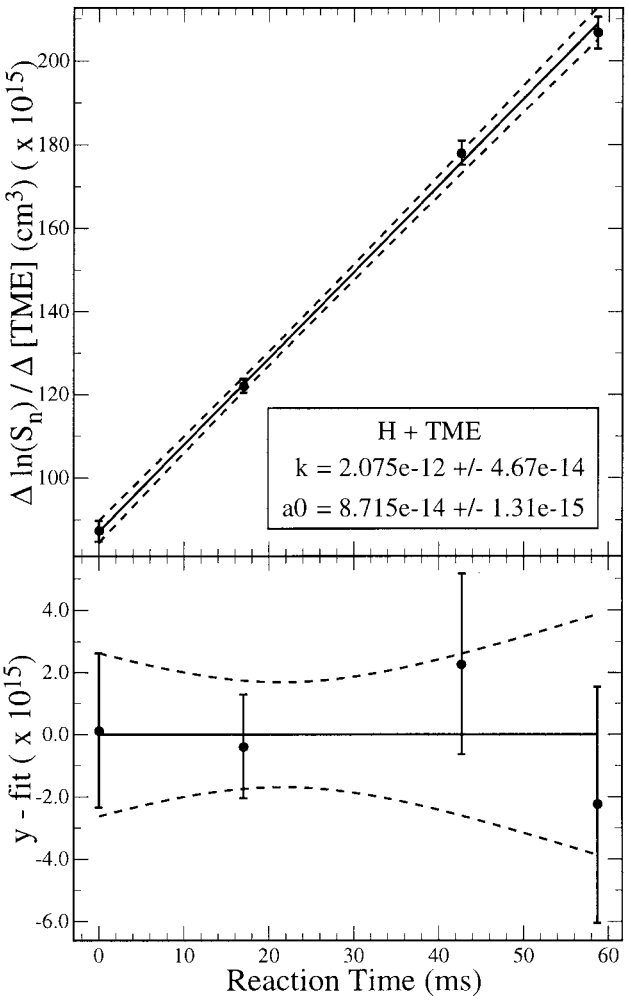

Figure 7. Slopes from Figure 6 versus reaction time (axis number). The lower panel shows the fit residuals with a 95% confidence interval, and the inset panel shows the fit results, including uncertainty, for the slope (*k*) and intercept (*a*0). Reaction time is defined as 0 at the first axis; the *x*-intercept (−42 ms in this case) approximately locates the point where the radical and reagent plumes mix.

$$H_3C\dot{C}H_2^* + M \rightarrow H_3C\dot{C}H_2 + M \qquad (8)$$

Such reactions exhibit a strong pressure dependence but reach an asymptotic high-pressure limit at a pressure that depends on the number of modes available to the adduct.

To investigate these pressure dependencies, we measured the room-temperature rate constants for H atom addition to ethene from 18 to 60 Torr, and to propene and *cis*-2-butene from 34 to 65 Torr. The data are shown in Table 1. Each reaction was measured a minimum of three times for each pressure. Over this pressure range, the rate constant of the H + ethene reaction increases by ∼30%, indicating a strong pressure dependence for this reaction at <60 Torr. Redissociation to reactants is competitive, with collisional stabilization of the adduct. Thus, the measured rate constant does not correspond exactly to passage over the addition barrier, and a barrier height cannot be easily extracted from temperature-dependent data.

The rate constants of H + propene and H + *cis*-2-butene, however, are constant over the range of pressures. This invariance is consistent with the studies of Kurylo et al.[37] and Harris and Pitts.[38] In comparison with the H + ethene reaction, these reactions have more complicated potential energy surfaces. In particular, decomposition of the adduct to products other than the reactants becomes possible, and in some cases there are

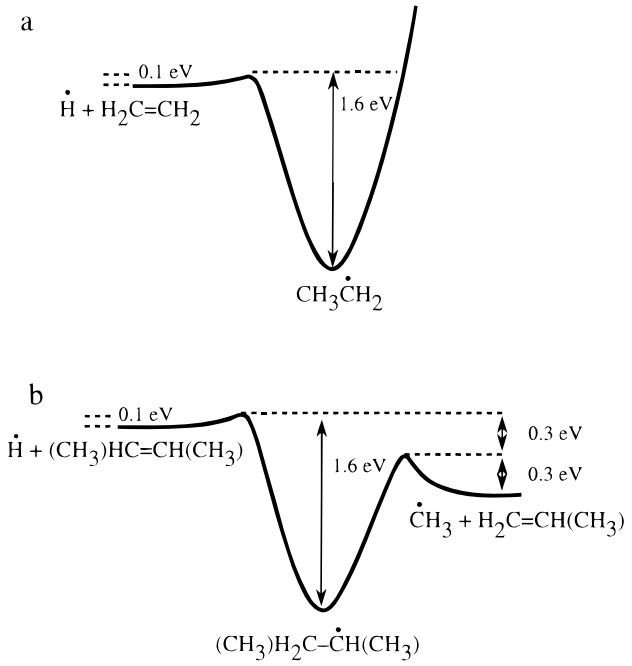

Figure 8. The potential energy surface for the reaction of H with (a) ethene and (b) *cis*-2-butene constrained by experiment. The reaction of H + ethene is strongly dependent on pressure; the adduct must be collisionally deactivated to the ethyl radical product. In the reaction of H + *cis*-2-butene, the second transition state is lower than the first. The first transition state is rate determining.

TABLE 1: Pressure-Dependent Data for the Reactions of H with Ethene, Propene, and *cis*-2-Butene ($\times 10^{-13}$ cm^3 molecule^{-1} s^{-1})

Pressure (Torr)	Ethene	Propene	*cis*-2-Butene
18.0	6.51 ± 0.16		
24.1	6.91 ± 0.05		
33.7	7.40 ± 0.27	16.0 ± 0.1	6.78 ± 0.06
40.9	7.89 ± 0.04		
50.2	8.10 ± 0.19	15.7 ± 0.1	6.79 ± 0.01
60.2	8.48 ± 0.13		
65.0		15.6 ± 0.3	6.88 ± 0.12

multiple reaction pathways. Although there is only one addition pathway (both π carbons are equivalent) for most compounds studied here, propene, isobutene, and 2-ethyl-1-butene have multiple pathways with radical attack strongly favored at the less-substituted carbon (see Harris and Pitts[38] and references therein). For example, H atoms can add to both the terminal and nonterminal π carbons of propene, resulting in two distinct adducts, *n*-propyl and *i*-propyl, respectively. Both adducts can be collisionally stabilized to products and can dissociate to reactants. However, because of the larger number of nonreactive modes, the lifetimes of these adducts are much longer than that of the ethyl adduct, thereby favoring collisional stabilization over dissociation. In addition, the *n*-propyl adduct can dissociate to a second set of distinct species; that is,

$$H_2C\dot{C}H_2CH_3^* \rightarrow CH_3 + H_2C=CH_2 \qquad (9)$$

The sole channel for H + *cis*-2-butene also has bimolecular products, as shown in Figure 8(b). The energies for the reactants, adduct, and products are again determined by heats of formation[32,33,39] whereas the barrier heights to reaction are constrained by temperature-dependent measurements (H + *cis*-2-butene from measurements described later; CH_3 + propene from Baulch et al.[40] For this potential energy surface, the free energy of the second transition state is substantially lower than the first, and there is no suggestion that it is substantially tighter; in such systems, the first transition state will be rate determining.[41−43] Although a full RRKM treatment of these reactive systems is beyond the scope of this work, the rate constants of the H + propene and H + *cis*-2-butene reactions should have little dependence on pressure at >15 Torr. For similar reasons, all other reactions considered here are at or near their high-pressure limits. Therefore, our measured rate constants correspond exactly to passage over the barrier to reaction, and we may easily determine a barrier height from temperature-dependent measurements.

Temperature Dependence. Temperature-dependent data for 12 of the reactions studied here are presented in Table 2 and shown in Figure 9. Each reaction was measured a minimum of seven times at each of four temperatures (298, 320, 345, and 370 K) and then averaged. The precision of these measurements is also presented. The accuracy of our data is ±10% (1σ) over the range of temperatures, and is primarily limited by the accuracy of our XS determination.

All data sets were fit to a modified Arrhenius expression.[15] This expression accounts for the curvature in Arrhenius plots due to the formation of loose vibrations between the H atom and the reactive site of the alkene at the transition state. For all reactions presented here, the following equation is used.

$$k(T) = \frac{B\, e^{(-E_a/T)}}{T^{1/2}\,(1 - e^{(-1.44 \times \nu_1/T)})\,(1 - e^{(-1.44 \times \nu_2/T)})} \qquad (10)$$

where ν_1 and ν_2 are taken to be 250 and 400 cm^{-1}, respectively, based on low-level ab initio calculations. Although these frequencies are expected to vary from reaction to reaction, the use of this function allows the temperature dependence in the preexponential to be treated explicitly, thereby giving a theoretically meaningful barrier height. These vibrations are the dihedral-angle bend between the H atom and the horizontal plane of the alkene, and the C−C−H bend between the H and C π system. The fit parameters are presented in Table 3.

Secondary Chemistry. One potential complication of these measurements is secondary chemistry involving the reaction products. If the energized adduct is stabilized to the alkyl radical (reaction 8), it can continue to react. Under experimental conditions where a large amount of alkyl radical is produced (i.e., high initial H atom concentrations), the following type of reaction can significantly influence the H atom decay:

$$H_3C\dot{C}H_2 + H \rightarrow \text{Products} \qquad (11)$$

Such reactions are quite fast for all of the systems studied here; for example, the rate constant of the H + ethyl reaction is $k_{298} = 6 \times 10^{-11}$ cm^3 molecule^{-1} s^{-1}.[40] The increase in decay of H atoms from a reaction such as this can result in an artificially high rate measurement for reaction 7. Therefore, we took great care to minimize the initial H atom concentration. In most experiments, $[H]_0$ was kept at $<3 \times 10^{10}$ molecules cm^{-3}, whereas H atom decay varied between 10 and 100 s^{-1}. Furthermore, the measured rate constants were invariant over a large range in $[H]_0$ [$(1-8) \times 10^{10}$ molecules cm^{-3}], suggesting that reaction 11 and other potential secondary reactions were not important under our experimental conditions.

Secondary radical removal can also be curtailed by adding a scrubber. In this case, we added O_2 to the system. At the relatively low temperatures of this experiment, oxygen will react with the initial alkyl radical ($k_{298} = 6.6 \times 10^{-12}$ cm^3 molecule^{-1} s^{-1} for the ethyl radical at 50 Torr)[9] to form peroxy radicals, that is,

TABLE 2: Averaged Rate Data for the Reaction of H with Alkenes and Haloalkenes at Four Temperatures ($\times 10^{-12}$ cm^3 molecule^{-1} s^{-1})

Compound	298 K	320 K	345 K	370 K
Propene	1.57 ± 0.01	1.98 ± 0.01	2.43 ± 0.02	2.98 ± 0.04
Isobutene	3.30 ± 0.01	3.70 ± 0.01	4.40 ± 0.03	4.87 ± 0.01
2-Ethyl-1-butene	3.92 ± 0.05	4.43 ± 0.02	5.10 ± 0.01	5.64 ± 0.05
cis-2-Butene	0.679 ± 0.007	0.924 ± 0.009	1.18 ± 0.04	1.51 ± 0.01
trans-2-Butene	0.825 ± 0.006	1.13 ± 0.01	1.52 ± 0.02	1.91 ± 0.03
2,3-Dimethyl-2-butene	1.34 ± 0.01	1.65 ± 0.01	2.01 ± 0.02	2.40 ± 0.03
Cyclopentene	1.23 ± 0.01	1.55 ± 0.03	1.96 ± 0.01	2.42 ± 0.01
Cyclohexene	0.923 ± 0.008	1.22 ± 0.01	1.56 ± 0.01	1.96 ± 0.01
3,4-Dimethyl-3-hexene	1.05 ± 0.01	1.33 ± 0.02	1.73 ± 0.06	2.14 ± 0.01
trans-1,2-Dichloroethene	0.122 ± 0.003	0.180 ± 0.002	0.247 ± 0.003	0.340 ± 0.005
1,2-Dibromoethene	0.0878 ± 0.0004	0.133 ± 0.005	0.190 ± 0.003	0.274 ± 0.004
Tetrachloroethene	0.0133 ± 0.0002	0.0215 ± 0.0001	0.0319 ± 0.0002	0.0476 ± 0.0002

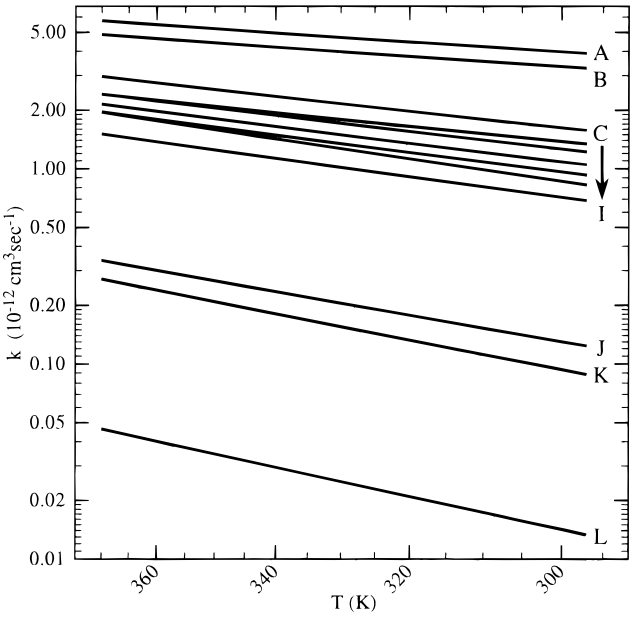

Figure 9. Modified Arrhenius plot for all reactions in this study. The following reactions are labeled: (A) 2-ethyl-1-butene, (B) isobutene, (C) propene, (D) 2,3-dimethyl-2-butene, (E) cyclopentene, (F) *cis*/*trans*-3,4-dimethyl-3-hexene, (G) cyclohexene, (H) *trans*-2-butene, (I) *cis*-2-butene, (J) *trans*-1,2-dichloroethene, (K) *cis*/*trans*-1,2-dibromethene, and (L) tetrachloroethene. Reactions C−I have similar room-temperature rate constants and Arrhenius functions.

TABLE 3: Fit Parameters for Each Reaction[a]

Alkene	B, 10^{-10} cm^{-3} s^{-1}	E_a, K
Propene	2.52 ± 0.14	812.6 ± 18.5
Isobutene	1.58 ± 0.13	457.1 ± 26.9
2-Ethyl-1-butene	1.77 ± 0.15	438.1 ± 28.3
cis-2-Butene	2.40 ± 0.14	1044.5 ± 20.4
trans-2-Butene	4.10 ± 0.34	1148.3 ± 26.5
2,3-Dimethyl-2-butene	1.66 ± 0.04	737.2 ± 7.2
Cyclopentene	2.49 ± 0.09	884.4 ± 12.6
Cyclohexene	2.62 ± 0.18	980.9 ± 23.5
3,4-Dimethyl-3-hexene	2.54 ± 0.06	936.4 ± 8.0
trans-1,2-Dichloroethene	1.31 ± 0.17	1372.9 ± 43.1
1,2-Dibromoethene	1.69 ± 0.21	1548.9 ± 39.6
Tetrachloroethene	0.478 ± 0.046	1736.0 ± 32.4

[a] See text; frequencies are held at 250 and 400 cm^{-1}.

$$H_3C\dot{C}H_2 + O_2 \rightarrow H_3CCH_2(OO) \qquad (12)$$

In sufficient quantities, the added oxygen inhibits reaction 11 by removing alkyl radicals before they can react with the atomic hydrogen. The measured rate constant was independent of O_2 concentration in the flow tube ($5 \times 10^{12} - 5 \times 10^{14}$ molecules cm^{-3}).

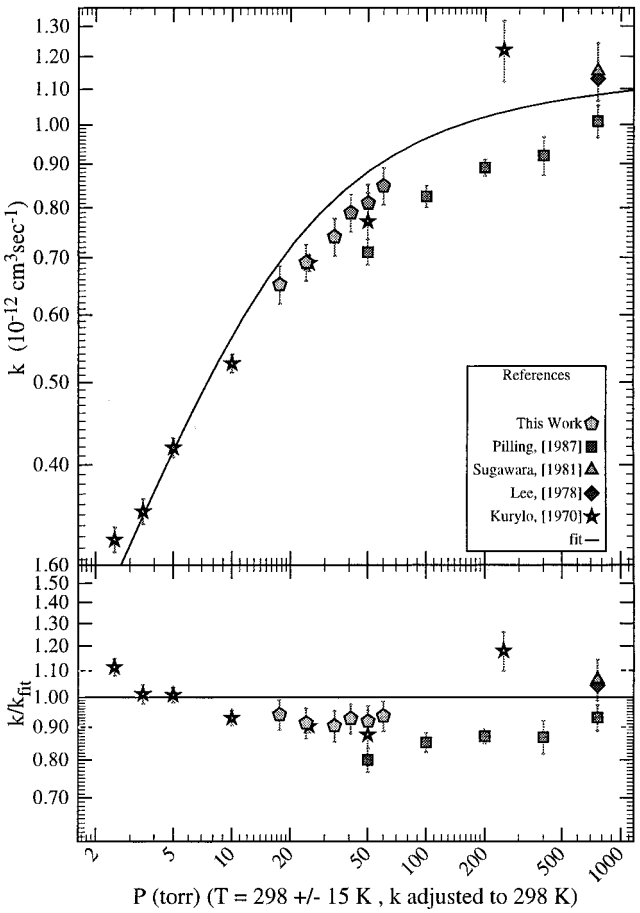

Figure 10. Logarithmic plot of the H + ethene → ethyl rate constant as a function of pressure. Other studies are indicated in the legend. Error bars for individual measurements are shown.

Literature Comparison

The literature for H atom additions to alkenes is sparse. For the reactions of H with 2-ethyl-1-butene, 2,3-dimethyl-2-butene, cyclopentene, 3,4-dimethyl-3-hexene, and also the haloalkenes, our data are the first absolute temperature-dependent measurements. In this section, data for the remaining reactions are compared with other published results.

For the reaction of H + ethene we fit our data and other data sets[34−36,44] to a simplified reduced falloff expression from Troe[9] (see Figure 10). All data are in good agreement, and the overall fit yields the following values at 298 K:

$$k_0(298) = (1.01 \pm 0.10) \times 10^{-29}\ \text{cm}^6\ \text{molec}^{-2}\ \text{s}^{-1} \qquad (13)$$

and

$$k_\infty(298) = (1.18 \pm 0.12) \times 10^{-12}\ \mathrm{cm^3\ molec^{-1}\ s^{-1}} \quad (14)$$

The value for k_∞ is in excellent agreement other published results.[34−36] An analysis using a more detailed reduced falloff expression would yield an even tighter fit, but even this simple analysis reproduces most of the observations to within 10%.

The temperature-dependent data for H + alkene reactions come primarily from two studies. Harris and Pitts[38] have studied the reactions of H with propene and the isomers of butene from 298 to 445 K using the flash photolysis technique, and Kyogoku et al.[45] have studied the reactions of H with the isomers of butene from 200 to 500 K using a pulsed-radiolysis technique. Comparisons of our data with each of these studies are shown for H + *cis*-2-butene (Figure 11) and H + isobutene (Figure 12). In general, our data are in better agreement with the data of Harris and Pitts. The data of Kyogoku et al. are substantially higher (30−60%) than our data over the 298−370 K temperature range and show smaller activation energies.

The temperature dependence of H + cyclohexene has also been measured directly by Hoyermann et al.[46] over the temperature range 296−493 K with an isothermal flow reactor. Their rate constants are lower than ours by 10−20%, but show a similar activation energy. This difference, however, is well within their given experimental uncertainty.

We cannot offer a critique of the earlier measurements; however, we stress that great care was taken to minimize potential sources of error in this experiment. Measured rates showed no dependence on a wide range of radical concentrations or on the presence of oxygen as a radical scrubber, indicating that secondary chemistry was not a problem under our experimental conditions.

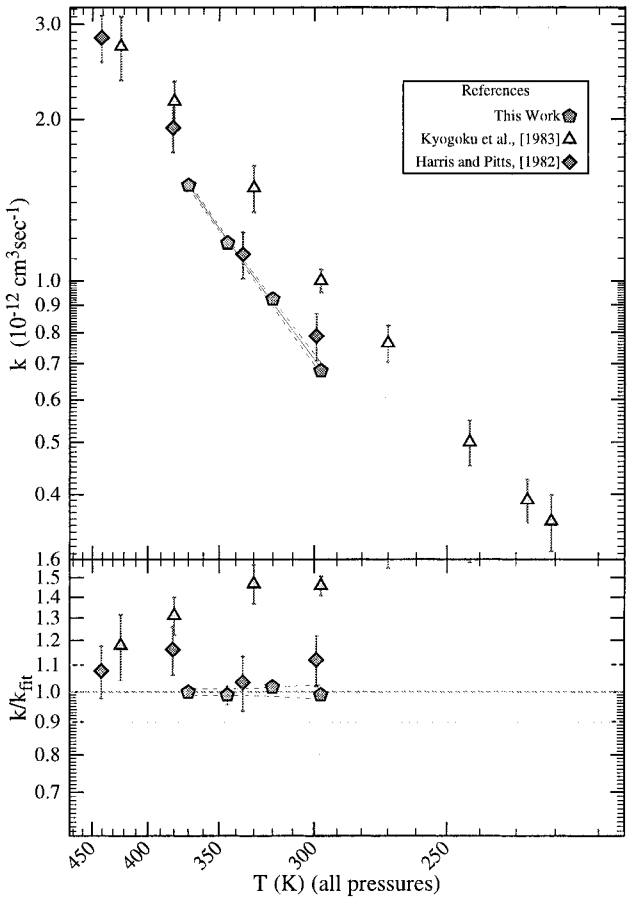

Figure 11. Rate constant, k, versus T for the reaction H + *cis*-2-butene → products. The temperature-dependent studies are indicated in the legend. Error bars for individual measurements are shown.

Discussion

The room-temperature rate constants for the reactions of H with alkenes and haloalkenes span almost 2.5 orders of magnitude, whereas the measured barrier heights change by a factor of 4. The alkenes in the three fastest reactions (lowest activation energies) have an unsubstituted π-bonded carbon; these are 2-ethyl-1-butene, isobutene, and propene. The alkenes of the three slowest reactions are halogenated. The remaining reactions with intermediate reactivity have similar room-temperature rate constants and activation energies.

The wide range of reactivity that these unsaturated compounds exhibit with H atoms must be explained by a molecular property evolving through the reaction series. The molecules studied here provide a diverse set of varying chemical properties, such as ionization potential, singlet−triplet splitting, and π-electron density. We chose the reaction set for two reasons: it appeared to have a good chance of lying near the transition from reactions dominated by excited ionic states to reactions dominated by singlet−triplet splittings, and it would be free of influence from far-field evolution in the ground state. However, above all else, we needed variability in rate constants and barrier heights for reactions measured at the high pressure limit. That need has clearly been met.

Conclusions

We have demonstrated a mathematically straightforward approach to analyzing rate data in the context of reactivity theories. One must identify key boundary conditions in a theory, calculate partial derivatives with respect to those boundary conditions, and then examine the actual variability in experimental data with respect to those derivatives. The particular power of this approach is that multiple correlated boundary conditions can be assessed simultaneously, revealing which parameter is actually controlling observed variability. In the relatively simple test case of H atom abstractions from alkanes by a series of radicals, we showed that the excited ionic state of the reactants is the controlling boundary condition; correlated and anticorrelated contributions from reaction enthalpy and product excited states are small and largely counteracting.

Having demonstrated the derivative technique, we measured a series of H atom additions to alkenes and haloalkenes in which the controlling physics is less well understood. These measurements required development of a more versatile experimental system than our original high-pressure flow system—one that permits easy study of not only a large molecular series of reactions, but equally easy study of movement from one radical to another. In this case, we expect competition between various excited states of the reactants and products, including both ionic and singlet−triplet excitations. To analyze these data we will have to develop a theoretical description of barrier height evolution amenable to the analysis technique described. Because of the more complicated excited-state landscape, such an analysis is beyond the scope of this work but will be presented in a forthcoming paper.[21] However, the technique is extensible; it exploits the power of the derivative to isolate parameters and motivates experiments designed to take advantage of its ability to break down complicated systems. The new experimental configuration is considerably more flexible than the first HPFS. The radical detection axes are designed to be interchangeable, allowing detection of atoms with RF, small radicals with LIF, and IR active species with cavity ringdown absorption after a

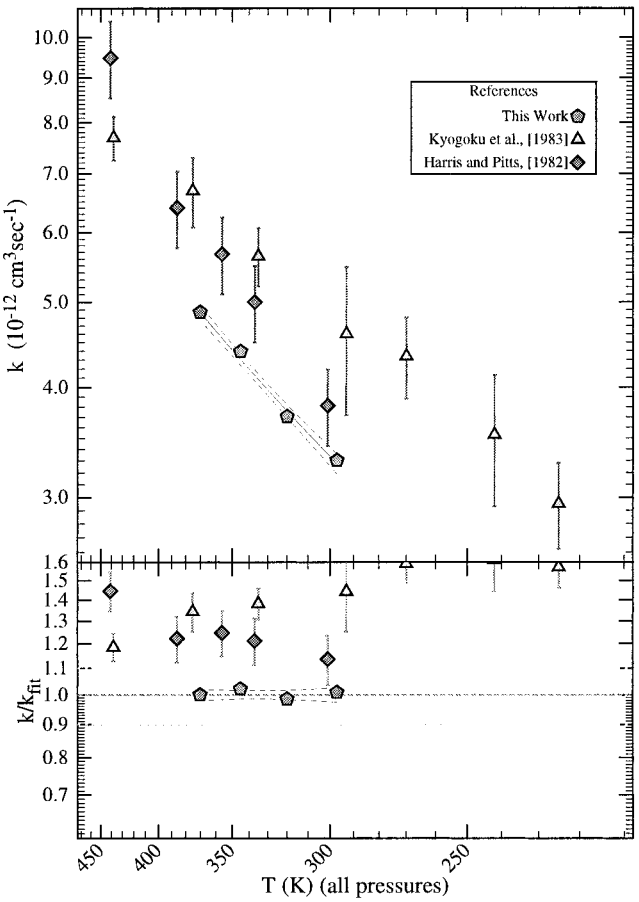

Figure 12. Rate constant, *k*, versus *T* for the reaction H + isobutene → products. The temperature-dependent studies are indicated in the legend. Error bars for individual measurements are shown.

minimum of reconfiguration. In addition, it is relatively small and easy to cool and heat over a wide temperature range, while remaining wall-less for pressures ranging from a few to a thousand or more torr. Future experiments will thus be designed to sequentially probe the aspects of the PES shown in Figure 1, continuing to reveal both what controls the PES and how reaction dynamics depends on it.

Acknowledgment. The authors thank Mike Greenberg, Jim Oliver, and Danny Spillane for assistance with the design and construction of the high-pressure flow system used in this work. This work was supported by NSF grant 9414843 to Harvard University.

References and Notes

(1) Giese, B. *Angew. Chem., Int. Ed. Engl.* **1983**, *22*, 753.

(2) Fossey, J.; Lefort, D.; Sorba, J. *Free Radicals in Organic Chemistry*; John Wiley and Sons: New York, 1995.

(3) Curran, D. P.; Porter, N. A.; Giese, B. *Stereochemistry of Radical Reactions: Concepts, Guidelines, and Synthetic Applications*; VCH Publishing: New York, 1995.

(4) Beckman, K. B.; Ames, B. N. *Physiol. Rev.* **1998**, *78*, 547.

(5) *Free Radicals in Biology*; Pryor, W. A., Ed.; Academic Press: New York. 1976.

(6) Francis, W.; Herron, J. T.; Cvetanovic, R. J. Compilation of chemical kinetic data for combustion chemistry. Technical Report 73-1, U. S. Department of Commerce, National Bureau of Standards, 1987.

(7) *Comprehensive Chemical Kinetics: Gas-Phase Combustion*, volume 17; Bamford, C. H.; Tipper, C. F. H., Eds.; Elsevier Scientific Publishing Company: New York, 1977.

(8) Albritton, D. L.; Watson, R. T.; Aucamp, P. J. Scientific assessment of ozone depletion. Technical Report 37, World Meteorological Organization, 1994.

(9) DeMore, W. B.; Sander, S. P.; Golden, D. M.; Hampson, R. F.; Kurylo, M. J.; Howard, C. J.; Ravishankara, A. R.; Kolb, C. E.; Molina, M. J. Chemical kinetics and photochemical data for use in stratospheric modeling. Technical Report 97-4, Jet Propulsion Laboratory, 1997.

(10) Seinfeld, J. H.; Atkinson, R.; Berglund, R. L.; Chameides, W. L.; Cotton, W. R.; Demerjian, K. L.; Elston, J. C.; Fehseneld, F.; Finlayson-Pitts, B. J.; Harriss, R. C.; Kolb, C. E.; Lioy, P. J.; Logan, J. A.; Prather, M. J.; Russell, A.; Steigerwald, B. Rethinking the ozone problem in urban and regional air pollution. Technical report, National Research Council, 1992.

(11) Atkinson, R. *J. Phys. Chem. Ref. Data* **1989**, *Monograph 1*, 246.

(12) Donahue, N. M.; Clarke, J. S.; Demerjian, K. L.; Anderson, J. G. *J. Phys. Chem.* **1996**, *100*, 5821.

(13) Clarke, J. S.; Kroll, J. H.; Donahue, N. M.; Anderson, J. G. *J. Phys. Chem.* **1998**, *102*, 9847.

(14) Donahue, N. M.; Dubey, M. K.; Mohrschladt, R.; Demerjian, K. L.; Anderson, J. G. *J. Geophys. Res.* **1997**, *102*, 6159.

(15) Donahue, N. M.; Demerjian, K. L.; Anderson, J. G. *J. Phys. Chem.* **1998**, *102*, 3121.

(16) Donahue, N. M. submitted for publication in *J. Phys. Chem.*

(17) Donahue, N. M.; Clarke, J. S.; Anderson. J. G. *J. Phys. Chem.* **1998**, *102*, 3923.

(18) Wong, M. W.; Pross, A.; Radom, L. *J. Am. Chem. Soc.* **1993**, *115*, 11050.

(19) Wong, M. W.; Pross, A.; Radom, L. *J. Am. Chem. Soc.* **1994**, *116*, 6284.

(20) Pross, A. *Theoretical and Physical Principles of Organic Reactivity*; John Wiley and Sons: New York, 1995.

(21) Clarke, J. S.; Rypkema, H. A.; Kroll, J. H.; Donahue, N. M.; Anderson, J. G. *J. Phys. Chem. A* **2000**, *104*, 4458.

(22) Silver, D. M. *J. Am. Chem. Soc.* **1974**, *96*, 5959.

(23) Shaik, S. S.; Hiberty, P. C. *Adv. Quantum Chem.* **1995**, *26*, 99.

(24) Atkinson, R. *J. Phys. Chem. Ref. Data* **1997**, *36*, 75.

(25) Abbatt, J. P. D.; Anderson, J. G. *J. Phys. Chem.* **1991**, *95*, 2382.

(26) Diaz-Acosta, I.; Alvarez-Idaboy, J. R.; Vivier-Bunge, A. *Int. J. Chem. Kinet.* **1999**, *31*, 29.

(27) Engels, B.; Peyerimhoff, S. D. *J. Phys. Chem.* **1989**, *93*, 4462.

(28) Engels, B.; Peyerimhoff, S. D.; Skell, P. S. *J. Phys. Chem.* **1989**, *94*, 1267.

(29) Abbatt, J. P. D.; Demerjian, K. L.; Anderson, J. G. *J. Phys. Chem.* **1990**, *94*, 4566.

(30) Weinstock, E. M.; Schwab, J. J.; Nee, J. B.; Schwab, M. J.; Anderson, J. G. *Rev. Sci. Instrum.* **1990**, *61*, 1413.

(31) Weinstock, E. M.; Hintsa, E. J.; Dessler, A. E.; Oliver, J. F.; Hazen, N. L.; Demusz, J. N.; Allen, N. T.; Lapson, L. B.; Anderson, J. G. *Rev. Sci. Instrum.* **1994**, *65*, 3544.

(32) Nicovich, J. M.; van Dijk, C. A.; Kreutter, K. D.; Wine, P. J. *J. Phys. Chem.* **1991**, *95*, 9890.

(33) Mallard, W. G. NIST chemical kinetics database. Technical Report 17, NIST, 1994.

(34) Lee, J. H.; Michael, J. V.; Payne, W. A.; Stief, L. J. *J. Chem. Phys.* **1978**, *68*, 1817.

(35) Sugawara, K.; Okazaki, K.; Sato, S. *Bull. Chem. Soc. Jpn.* **1981**, *54*, 2872.

(36) Lightfoot, P. D.; Pilling, M. J. Temperature and pressure dependence of the rate constant for the addition of H to C_2H_4. *J. Phys. Chem.* **1987**, *91*, 3373.

(37) Kurylo, M. J.; Peterson, N. C.; Braun, W. *J. Chem. Phys.* **1971**, *54*, 4662.

(38) Harris, G. W.; Pitts, J. N. Absolute rate constants and temperature dependences for the gas-phase reactions of H with propene and the butenes in the temperature range 298 to 445 K. *J. Chem. Phys.* **1982**, *77*, 3994.

(39) Seakins, P. W.; Pilling, M. J.; Niiranen, J. T.; Gutman, D.; Krasnoperov, L. N. Kinetics and thermochemistry of R + HBr ⇌ RH + Br reactions: Determinations of the heat of formation of C_2H_5, *i*-C_3H_7, *sec*-C_4H_9, and *t*-C_4H_9. *J. Phys. Chem.* **1992**, *96*, 9847.

(40) Baulch, D. L.; Cabos, C. J.; Cox, R. A.; Esser, C.; Frank, P.; Just, T.; Kerr, J. A. *J. Phys. Chem. Ref. Data* **1992**, *21*, 411.

(41) Mozurkewich, M.; Benson, S. W. *J. Phys. Chem.* **1984**, *88*, 6429.

(42) Patrick, R.; Barker, J. R.; Golden, D. M. *J. Phys. Chem.* **1984**, *88*, 128.

(43) Kircher, C. C.; Sander, S. P. *J. Phys. Chem.* **1984**, *88*, 2082.

(44) Kurylo, M. J.; Peterson, N. C.; Braun, W. *J. Chem. Phys.* **1970**, *53*, 2776.

(45) Kyogoku, T.; Watanabe, T.; Tsunashima, S.; Sato, S. *Bull. Chem. Soc. Jpn.* **1983**, *56*, 19.

(46) Hoyermann, K.; Preuss, A. W.; Wagner, H. G. *Ber. Bunsen-Ges. Phys. Chem.* **1975**, *79*, 156.